

Article

A Study of Respirable Silica in Underground Coal Mines: Particle Characteristics

Cigdem Keles * and Emily Sarver 

Mining & Minerals Engineering, Virginia Polytechnic Institute and State University, Blacksburg, VA 24061, USA

* Correspondence: cigdem@vt.edu

Abstract: Respirable crystalline silica is now considered to be a major culprit of resurgent lung disease among US coal miners—especially in central Appalachia—though questions remain regarding the specific circumstances around exposure to it. As part of a larger investigation of dust in 15 US coal mines, a recent study examined the silica content in both the respirable mine dust samples and the samples of respirable dust generated in the laboratory from primary source materials (i.e., coal and rock strata and rock dusting products). It concluded the rock strata that is being drilled for roof bolting or is being cut along with the coal is the most significant source of respirable silica in many mines, which is consistent with the expectations based on other scattered datasets. However, little information is available on the characteristics of respirable silica particles which might be important for understanding the exposure risks better. In the current study, which represents another part of the aforementioned investigation in 15 mines, scanning electron microscopy with energy dispersive X-ray spectroscopy (SEM–EDX) were used to analyze the size and surface condition (i.e., degree of surface-associated clay) of 1685 silica particles identified in 58 respirable mine dust samples. The results indicated that silica is typically finer in locations nearby to drilling and cutting activities than it is in other locations within a mine, but the silica in the Central Appalachian mines is not necessarily finer than it is in the mines in other regions. An analysis of the particle surfaces revealed that respirable silica in coal mines often does not occur as “free”, high-purity particles. Rather, there can be a range of occurrences including silica particles having a thin “occlusion” layer of clay, silica within agglomerates that can also contain other particle types including clays, or even silica ingrained within other particles such as coal.

Keywords: respirable crystalline silica (RCS); respirable coal mine dust (RCMD); scanning electron microscopy with energy dispersive X-ray spectroscopy (SEM–EDX); particle size; particle surfaces



Citation: Keles, C.; Sarver, E. A Study of Respirable Silica in Underground Coal Mines: Particle Characteristics. *Minerals* **2022**, *12*, 1555. <https://doi.org/10.3390/min12121555>

Academic Editor: Jordi Ibanez-Insa

Received: 21 October 2022

Accepted: 28 November 2022

Published: 1 December 2022

Publisher’s Note: MDPI stays neutral with regard to jurisdictional claims in published maps and institutional affiliations.



Copyright: © 2022 by the authors. Licensee MDPI, Basel, Switzerland. This article is an open access article distributed under the terms and conditions of the Creative Commons Attribution (CC BY) license (<https://creativecommons.org/licenses/by/4.0/>).

1. Introduction

The prevalence of occupational lung disease among US coal miners has been on the rise since the late 1990s, particularly in Central Appalachia [1–3]. In many cases, the disease is severe and rapidly progressive with there being radiographic [4,5] and pathologic evidence that implicates silica exposure [6–8]. However, the available dust monitoring data from mines cannot readily explain the recent resurgence of the disease [9,10]. In fact, the data gathered for regulatory compliance assessments indicate generally downward trends in the mass concentration of respirable coal mine dust (RCMD) and the percentage of samples exceeding the permissible exposure limit for quartz (i.e., the dominant form of crystalline silica) [11]. As such, there has been a lot of speculation that the changes in the RCMD characteristics might be a factor in the resurgence of disease. With respect to silica, specifically, the size (e.g., [12–15]) and surface features of the particles [16–18] could be important, though neither has been widely explored in the mine environment.

The mechanisms of respirable silica toxicity and disease pathology have been the subject of significant research (e.g., as reviewed by [19–23]). With respect to particle size, finer silica is expected to enhance the response by the alveolar macrophages, which is

widely accepted as the first step in a proinflammatory and self-propagating process that can ultimately lead to pulmonary fibrosis [12,18,19]. Fundamentally, the enhanced effect of fine silica is probably due to its increased surface area or total particle number per unit mass with decreasing size [12] and/or its ability to penetrate further into the lungs [14]. As mining equipment has become more powerful and the mines, especially in Central Appalachia, have tended to cut more rock along with the coal (i.e., in “thin seam” mines), it stands to reason that the abundance of fine silica particles in the mine environment might have increased over the past decades [9]. While standard quartz content analysis (e.g., by MSHA Methods P7 or P2, or NIOSH Methods 7500 or 7603) of size-segregated samples can be used to evaluate the mass distributions of respirable silica in mine dust (e.g., [24–26]), an analysis of the individual particles can enable a better understanding of the finest and perhaps most hazardous dust constituents. For this, scanning electron microscopy with energy dispersive X-ray (SEM–EDX) can be applied to RCMD samples to count, size and classify the particles [27,28].

In addition to the size, the surface features of the silica particles are likely important factors for controlling the severity of the lung response [19,29,30]. Based on the surface features, the silica could be either free silica (i.e., pure silica) or it might have some impurities and be covered with a thin clay (i.e., aluminosilicate mineral) layer, which are called occluded silica particles. Freshly fractured particles, as might be expected in newly generated mine dust, should have a relatively higher abundance of reactive oxygen species than the aged particles would have, and they have been associated with more severe inflammation and lung injury [17,31–36]. On the other hand, silica particles occluded with a thin layer of clay as opposed to “free” silica have been associated with less severe outcomes in both the laboratory and epidemiological studies [18,37–43]. Following up on research that correlated an earlier prevalence of occupational lung disease in US coal miners with a higher coal rank [44], the US National Institute for Occupational Safety and Health used SEM–EDX to conduct several studies to evaluate the surface condition of the silica particles in RCMD; they found that the relative fraction of occluded (versus free) silica was generally lower in the mines with a higher coal rank [45–47]. However, the role of silica surface occlusion—or lack thereof—in the context of the recent disease resurgence among US coal miners has not been extensively studied. Preliminary work by Frost et al. [48] suggested that the fraction of occluded or free silica might be related to the specific source of respirable silica in the mine environment.

As part of a larger investigation of dust in 15 US mines, a recent study by the authors looked at the sources of respirable silica [49]. Using multiple analytical methods (i.e., scanning electron microscopy with energy dispersive X-ray spectroscopy, Fourier transform infrared spectroscopy and the standard NIOSH 7603 method), the silica content was determined in the RCMD samples (collected at various locations of each mine). In addition, the silica content was determined in the respirable samples generated in the laboratory from primary dust-source materials, including the target coal seam and surrounding rock strata being mined at the face, the roof rock strata being drilled for bolting, and the rock dust products being applied in the mine to mitigate the explosibility hazards, which should contain less than 4% free and combined silica as per US regulation (see CFR-Title 30 [50]). The results indicated that the rock strata encountered during drilling or mining is typically the most significant source of respirable silica, although the silica might also be sourced from the coal seam in some mines. As another part of this 15-mine investigation, the current work explores the characteristics of the silica particles contained in the RCMD. Here, SEM–EDX work was conducted on 58 samples, from which 1685 individual silica particles were evaluated in terms of their surface condition (i.e., the presence of surface-associated clay) and size. Additional context was drawn from a pre-existing dataset of 171 samples (including the above 58) that could be used to evaluate the size distribution of silica relative to other particle types.

2. Materials and Methods

2.1. Available RCMD Samples

As reported by Keles et al. [49], a total of 75 RCMD samples from 15 US underground mines were already analyzed for their silica mass content, and these samples were also available for the current study. (It is noted that these samples from 15 mines are actually part of a wider sample inventory covering 25 mines. Sarver et al. [51] analyzed that entire inventory to broadly investigate the dust mineralogy and size distributions, and the comprehensive dataset is now publicly accessible (see Keles et al. [52]). However, as explained by Keles et al. [48], to specifically investigate the silica, the focus was limited to just 15 mines from which bulk samples of primary dust-source materials were also available—i.e., in addition to the RCMD samples.) The 15 mines represent four distinct geographic regions: Central Appalachia (CA), Northern Appalachia (NA), the mid-west/Illinois basin (MW) and the western basin (W). In each mine, the sampling targeted five standardized locations: the intake airway to a producing mine section (I), an area adjacent to the feeder breaker (F), an area just downwind of the active production face (P), an area just downwind of an active roof bolter (B), and an area in the return airway (R). Schematic diagrams illustrating approximate sampling locations for RCMD samples are illustrated in Figure S1 in the Supplementary Materials. Since the aim of the current study was to investigate the silica particle characteristics, data from the prior SEM–EDX analysis were used to screen out the samples that had less than 2% silica (based on particle counts); this reduced the total number of samples to 58 (Table 1).

Table 1. Summary of available RCMD samples from 15 underground coal mines. (Modified from Keles et al. [48].)

Mine	Mine	MSHA	State ²	Mining	Coal	Mining	Roof	Sampling Location ⁵					Total	
	reg. ¹	District		Method ³	Ht. (m)	Ht. (m)	Strata ⁴	B	P	R	F	I		
10	CA	5	KY	CM	1–1.2	1.8–1.9	Sh/Sn	2	0	1	2	1	6	
11	CA	5	VA	CM	0.8	1.2–1.3	Sh	1	1	1	1	0	4	
12	CA	5	VA	CM	0.8–1.5	1.9–2.0	Sh/Sn	1	1	1	0	1	4	
13	CA	5	VA	LW	1.5–1.8	1.8–2.0	Sn/Sh	0	0	1	1	2	4	
14	CA	5	VA	CM	0.6–0.9	1.5–1.9	Sh	1	0	0	1	1	3	
15	CA	4	WV	CM	0.9–1.2	2	Sh	1	1	1	0	0	3	
16	NA	3	WV	CM	2.7	2.1	Sh	1	1	1	1	0	4	
17	NA	3	WV	LW	1.5–1.8	2.0–2.3	Sh	1	1	2	0	2	6	
18	NA	3	WV	CM	0.7–0.8	1.5–1.8	Sh	1	1	1	1	1	5	
19	MW	8	IL	CM	1.8–2.0	1.9–2.3	Sh/Lm	1	1	2	1	1	6	
20	MW	8	IL	CM	1.8–1.9	1.8–2.0	Sh/Lm	1	0	0	2	1	4	
21	CA	12	WV	CM	0.8–1.0	2	Sh/Sn	1	0	1	1	1	4	
22	CA	12	WV	CM	0.8	1.4	Sh	0	1	0	1	0	2	
23	W	9	CO	LW	6.1	4.3	Sh	0	0	0	0	0	0	
24	W	9	CO	LW	1.8	2.1–2.4	Sh/Sn	0	0	1	1	1	3	
								B	P	R	F	I	Total	
								Total	12	8	13	13	12	58

¹ Mine region: CA = Central Appalachia; NA = Northern Appalachia; MW = mid-west; W = west. ² State: KY = Kentucky; VA = Virginia; WV = West Virginia; IL = Illinois; CO = Colorado. ³ Mining method: CM = continuous miner; LW = longwall. ⁴ Roof strata: Description based on observations during RCMD sampling. Sh = shale; Sn = sandstone; Lm = limestone. ⁵ Sampling location: I = intake; R = return; P = production; B = roof bolter; F = feeder breaker.

The RCMD sample collection and the preparation procedures for the SEM–EDX work are detailed in Keles et al. [48]. Briefly, the samples were collected directly onto 37 mm polycarbonate filters (track etched, 0.4 µm pore size) in two-piece cassettes using Escort ELF air sampling pumps operated at 2 L/min with 10 mm nylon Dorr-Oliver cyclones to collect only the respirable-sized particles. The sampling time was generally 2–4 h in all of the locations. Following the collection, the samples were transported to Virginia Tech ICTAS-NCFL lab and prepared for analysis. A circular subsection (8–9 mm) was carefully cut using a stainless-steel trephine. The particle deposition was higher at the center for the heavily loaded samples. If the dust loading on the filter appeared to be high, the subsection

was cut off-center (i.e., the subsection was cut outward toward the edge of the filter) to minimize the particle loading density (PLD) under SEM. Each subsection was mounted on a pre-labeled aluminum stub and sputter coated with gold/palladium for 1 min. Sputter coating is necessary to reduce the microscope beam damage and sample charging, improve secondary electron emission and protect the sample during handling [53].

2.2. Silica Particle Surface Analysis

To analyze the surface condition of the silica particles in the 58 RCMD samples included here, an SEM–EDX method was applied, which Harrison et al. [44,54] used to evaluate respirable particle silica occlusion by an aluminosilicate clay layer. The method had been previously described by Wallace et al. [55] and patented by Wallace and Keane [56], and it was also validated by Hnizdo and Wallace [57]. In short, it involves analyzing a silica particle at two different accelerating voltages (i.e., 20 and 5 kV) and determining the change in the silicon and aluminum ratios (i.e., $Si/(Si + Al)$) as a function of the change in voltage. The basic premise is that the $Si/(Si + Al)$ ratio should decrease significantly from 20 to 5 kV for the occluded silica particles—or particles that have surface-associated clay, more generally—but it should not change much for the free silica particles [55]. This is because the higher voltage electron beam should penetrate into the core of the silica particle and produce elemental spectra accordingly, whereas the spectra produced at the lower voltage should be more influenced by the particle surface (see Figure 1).

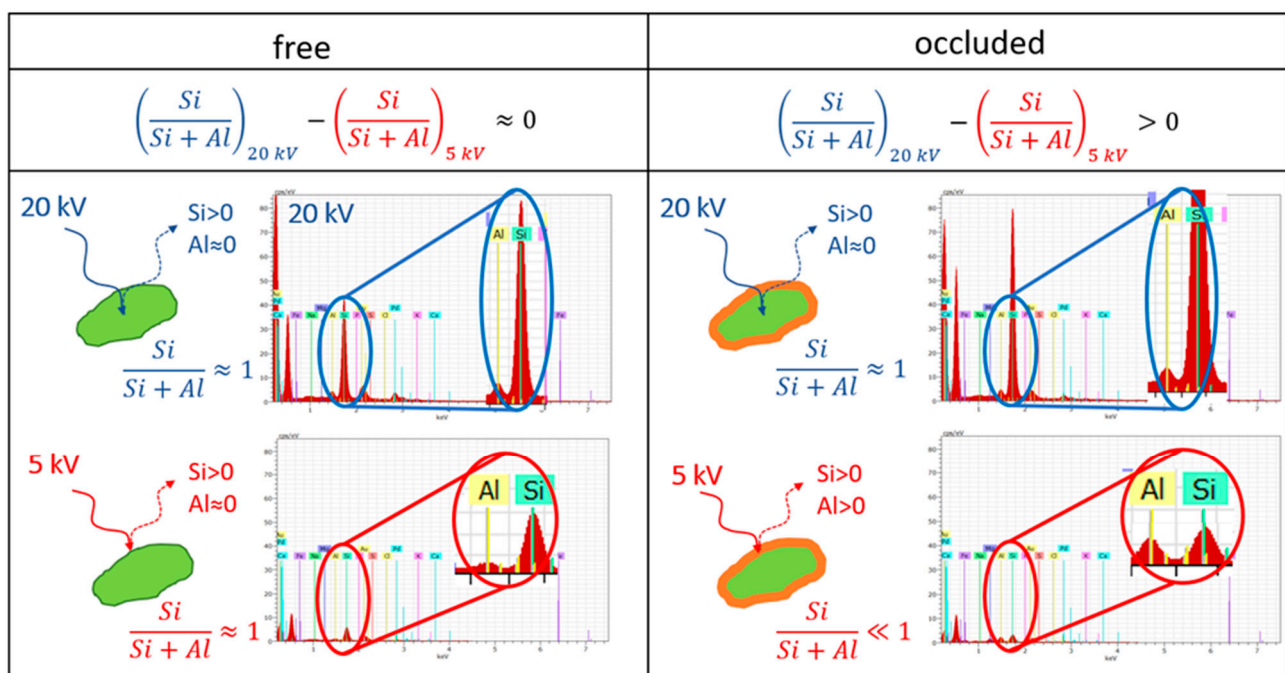


Figure 1. Conceptual illustration of SEM–EDX analysis on free versus “occluded” silica particles at relatively high (20 kV) and low (5 kV) accelerating beam voltages.

The next sections describe the procedures used in the current study to identify and analyze individual particles at two voltages by SEM–EDX and to establish the classification criteria for free silica (versus silica with surface-associated clay) using reference particles.

2.2.1. Particle Identification and Dual-Voltage Analysis

All of the SEM–EDX work for the analysis of the silica particle surface was performed using an FEI Quanta 600FEG Environmental SEM (Hillsboro, OR), which was equipped with a backscatter electron detector (BSD) and a Bruker Quantax 400EDX spectroscope (Ewing, NJ, USA), and using Bruker’s Esprit software (version 1.9.4). The instrument was

operated under a high vacuum condition, with a 12.5 mm working distance, a 5.5 μm spot size, 5000 \times magnification, 92.5% brightness, and 60%–70% contrast.

The analysis of each RCMD sample was completed using a two-step procedure as illustrated in Figure 2. The first step served as a sort of rapid screening of the sample. It involved using a computer-controlled (CC) routine (developed specifically for the current study) to identify and locate the silica particles at 15 kV. (This voltage was chosen to be consistent with the SEM–EDX work that was previously performed on these and other samples to generate a large particle size and mineralogy distribution dataset [52], which is discussed further below). The aim was to find up to 50 silica particles per sample in the length range of 0.5–5 μm . The CC routine achieved this by scanning the first 30 particles (from left to right and from top to bottom) in a field of view (“frame”) and collecting data on their size and EDX spectra, from which the normalized atomic percentage of eight elements was determined (C, O, Al, Si, Mg, Ca and Ti). The particles in the desired size range and with an Si/(Si + Al) ratio ≥ 0.70 were classified as silica; this is a conservative approach and might exclude silica particles with the most pronounced clay influence (e.g., small silica particles with a thick clay layer, which are included in agglomerates with many clay particles or that are surrounded by many clay particles due to high filter loading). After each frame was analyzed, the CC routine moved on to another frame until a total of 50 silica particles had been identified and located (i.e., by their x and y coordinates) or until 100 frames or 1000 total particles had been analyzed. The frame locations were pre-programmed to ensure that a wide area of the sampled filter was scanned, and hence, representative data were collected. For efficiency, the elemental data were not saved for the particles that were not classified as silica, and the images and elemental maps were only captured periodically. However, the observed PLD was recorded for each sample as a measure of the total number of particles per analyzed filter area ($\#/\mu\text{m}^2$). As discussed by Keles et al. [49], PLD can be important for the SEM–EDX analysis of individual particles since high loading can cause interference between the particles.

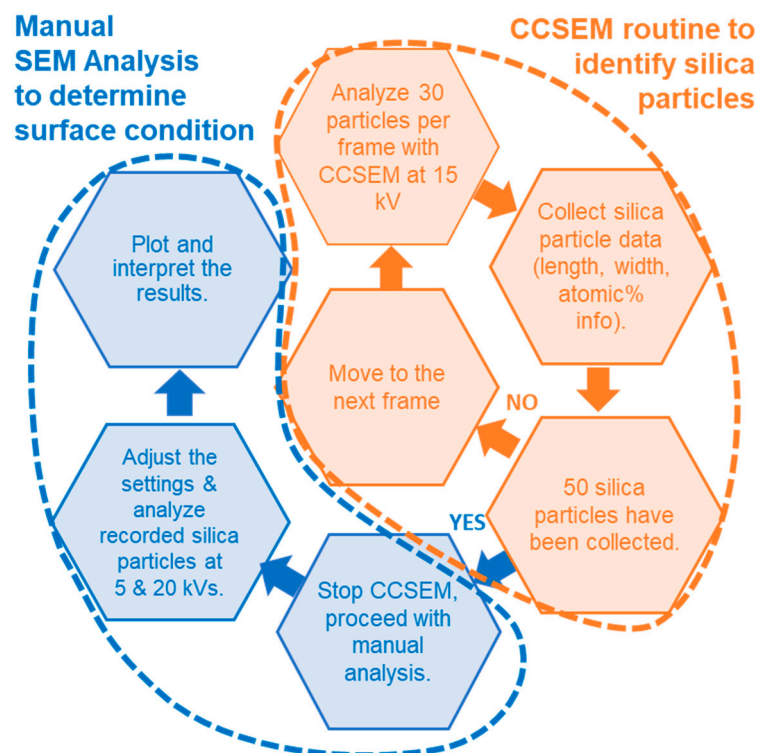


Figure 2. Two-step procedure for SEM–EDX analysis of silica particle surface condition.

The second step of the procedure involved manually revisiting each of the silica particles that had been identified and located by the above CC routine. For each particle,

the EDX spectra were again obtained at 20 and 5 kV from the particle center with point analysis. The Si/(Si + Al) ratio was computed for both of the voltages, and then, the change in that ratio was recorded as the difference between the values at 20 and 5 kV.

2.2.2. Reference Material Selection

To establish the range of the Si/(Si + Al) ratios that might be exhibited by the free silica particles, and thus, the threshold values for the change in this ratio between 20 and 5 kV that could be used to distinguish the free silica from the silica with surface-associated clay, it was necessary to characterize the particles in a suitable control material. Consistent with the seminal work by Harrison et al. [44], the key criteria for such reference particles were: (1) They must have a high silicon content (i.e., $\text{Si}/(\text{Si} + \text{Al}) \geq 0.70$), such that the particles are elementally similar to those classified as silica by the SEM–EDX routine. (2) They should have a low-level, but homogeneous, aluminum content. This is important because in contrast to a pure silica particle (i.e., a negligible aluminum content), the objective is to observe how the ratio of Si and Al changes from the particle core (i.e., at 20 kV) to the surface (i.e., 5 kV). If a particle has virtually no aluminum, its Si/(Si + Al) ratio is theoretically 1.0 at both of the voltages, and the change in the ratio will of course be minimal. If a particle has some homogeneous aluminum contamination, its change in the Si/(Si + Al) ratio should still be minimal since the Al is uniformly dispersed through the particle; however, its Si/(Si + Al) ratio $\neq 1.0$ at either 20 or 5 kV. This means that any potential bias in the EDX data as the voltage is varied can be evaluated and accounted for in the established thresholds for distinguishing the free silica from the silica particles with surface-associated clay.

Based on the above two criteria, a fused aluminosilicate glass powder (“VCAS160”; Vitro Minerals, Jackson, TN, USA) was selected to generate the free silica control particles. This material was expected to have a high Si/(Si + Al) ratio, with the minor aluminum content being contained homogeneously. Four other materials were also used to generate reference particles to validate the free silica classification: Min-U-Sil 5 and Sil-Co-Sil (US Silica, Katy, TX, USA) were used as a source of pure crystalline silica (i.e., $\text{Si}/(\text{Si} + \text{Al})_{20\text{ kV}} \approx \text{Si}/(\text{Si} + \text{Al})_{5\text{ kV}} \approx 1.0$, so minimal change in the ratio was expected), the silica particles found in ball clay Kentucky stone (The Ceramic Shop, Norristown, PA, USA) were used as a source of clay-occluded silica particles (i.e., $\text{Si}/(\text{Si} + \text{Al})_{20\text{ kV}} > \text{Si}/(\text{Si} + \text{Al})_{5\text{ kV}}$, so positive change in the ratio was expected, and kaolinite (Ward’s Science, Rochester, NY, USA) was used as source of pure aluminosilicate particles (i.e., $\text{Si}/(\text{Si} + \text{Al})_{20\text{ kV}} \approx \text{Si}/(\text{Si} + \text{Al})_{5\text{ kV}} < 1.0$, so minimal change in the ratio was expected).

To generate the dust samples from each reference material, the material was aerosolized in a small enclosure and the equipment identical to that described for the RCMD sampling was used to collect the respirable particles directly only using the PC filters in two-piece cassettes. Subsections of the filters were then prepared for the SEM–EDX analysis sputter coating, and the analysis was conducted per Figure 2.

2.2.3. Classification Criteria for Free Silica

Figure 3a shows the Si/(Si + Al) ratio at each voltage, and Figure 3b shows the change in the Si/(Si + Al) ratio from 20 to 5 kV for the respirable particles collected from the reference materials. As expected, the control particles (i.e., $n = 50$, from VCAS160) exhibited similar Si/(Si + Al) ratios at both of the voltages, with values mostly at 0.75–0.80. Moreover, the change in the Si/(Si + Al) ratio from 20 and 5 kV was relatively small. The other reference particles also behaved as expected. The particles from the pure silica materials generally had Si/(Si + Al) ratios near 1.0 at both of the voltages, whereas those from the pure kaolinite had ratios near 0.40–0.45 at both of the voltages. In both of the cases, this yielded virtually no change in the ratio from 20 to 5 kV. However, the silica particles from the ball clay exhibited the characteristic positive change in the ratio predicted for the clay-occluded silica. (i.e., $(-0.038, 0.036)$).

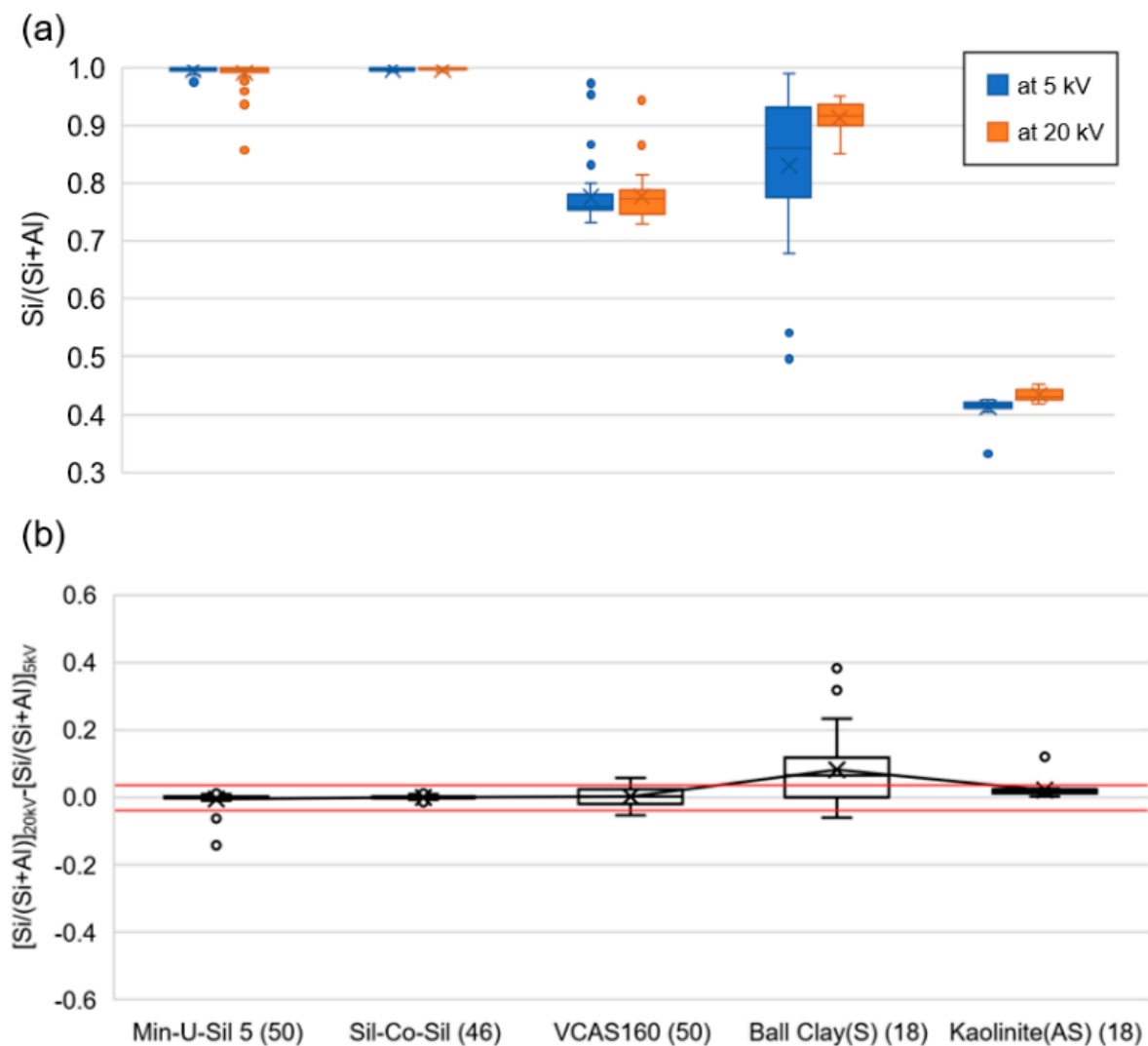


Figure 3. (a) Distribution of the Si/(Si + Al) ratio at 5 and 20 kV and (b) distribution of the change in Si/(Si + Al) ratio from 20 to 5 kV for respirable particles collected from reference materials. The number of analyzed silica particles (or aluminosilicate particles for kaolinite) are given in parentheses. Red lines represent the 5th and 95th percentiles determined from the VCAS160 reference particles (i.e., [−0.038, 0.036]). Small circles are the outliers.

To establish the thresholds for free silica classification, the 5th and 95th percentiles for the change in Si/(Si + Al) from 20 to 5 kV were calculated using the data from the VCAS160 control particles (see red lines in Figure 3b). By definition, 90% of the VCAS160 particles fell within these bounds. (Consistent with the above remarks, the particles from the other pure or homogeneous reference materials did as well). Accordingly, for the evaluation of the silica particles with unknown surface condition in the current study, if a particle exhibited a change in the Si/(Si + Al) ratio within these bounds (i.e., [−0.038, 0.036]), it was considered to be free silica.

2.3. Silica Particle Size Analysis

In the current work, the silica particle size was evaluated on the basis of the particle length (i.e., longest dimension measured in SEM–EDX analysis), and two sources of data were used as described below.

2.3.1. Data from Silica Particle Surface Analysis

During the first step of the silica particle surface analysis on the 58 RCMD samples shown in Table 1, length measurements of each particle identified as silica were collected using the CC SEM–EDX routine, and then, each particle was revisited for the manual dual-voltage analysis. Thus, the size and surface classification could be directly correlated per particle.

2.3.2. Pre-Existing Data

The silica particle size distribution data were also available from a previous SEM–EDX analysis of the wider RCMD sampled set mentioned above, which included the 58 samples that were further analyzed for the current study. The wider sample set has a total of 171 samples from 25 mines (i.e., collected from the five standardized sampling locations shown in Table 1); after accounting for the cases where multiple samples were collected in the same location in a single mine, or no samples could be collected in a particular location of a mine, the wider set represents 106 unique sampling locations (i.e., mine \times location). All of the 171 samples were previously analyzed by SEM–EDX to investigate the particle size and mineralogy distributions [51]. Briefly, that analysis covered the entire size range of 0.1–10 μm , and the particles were sorted by their EDX spectra into predefined mineralogy classes, which predominantly included: carbonaceous (C), mixed carbonaceous (MC), aluminosilicates (AS), silica (S) and carbonates (CB). The work was completed using two computer-controlled (CC) routines (i.e., one was for submicron, and one was for supramicron particles) with the same instrumentation and software as used here for the silica particle surface analysis. Details of both of the routines, as well as the method used to merge their data, are given in [51]. The final output of that analysis included the particle size distributions for each mineralogy class on a per sample basis [52]. Thus, the pre-existing dataset can be used to evaluate the size distributions for the silica relative to other types of particles (i.e., which was not possible with the dataset yielded by the procedure shown in Figure 2). Here, those previous results were truncated to only include particles in the range of 0.5–5 μm to be consistent with the data collected for the silica particle surface analysis.

3. Results and Discussion

Table 2 summarizes the results of the SEM–EDX analysis that was conducted on 58 RCMD samples for the current study (i.e., per Figure 3). The results are presented in terms of the number of respirable silica particles analyzed, the mean particle length, and the mean change in the Si/(Si + Al) ratio from 20 to 5 kV, and the results are organized by sampling location and mine region. (The individual particle data for each sample are available in Table S1 in the Supplementary Materials). As mentioned earlier, an excessive PLD on the sample filter can cause interference between the particles, so for the current work, if a silica particle was sitting in close proximity to Al-rich particles (i.e., aluminosilicate clays), this situation could cause the particle to be missed by the CC silica identification routine or to exhibit an increased Al content during the manual SEM–EDX analysis at two voltages. Thus, the results in Table 2 are presented separately for the samples with a low versus high observed PLD. Per the recent study by Keles et al. [48], a PLD threshold of 0.035 $\#/\mu\text{m}^2$ was used, which yielded 46 samples in the low PLD group and 16 samples in the high PLD group. The samples from the production (P) location were more likely to have a high PLD, which is attributed to the relatively higher dust concentration in this area of the mine (i.e., the samples were collected just downwind of the active mining); likewise, some of the roof bolter (B) and return airway (R) samples were also affected, and these locations also tended to have higher dust concentrations than the feeder breaker (F) and intake airway locations (I) did [58]. That being said, there was no indication that a high PLD necessarily affected the size of the silica particles that could be identified for the analysis (see Figure S2 in for plot of silica particle length versus observed PLD).

Table 2. SEM–EDX silica analysis results summarized by sampling location and mine region.

Mine Region ¹	Sampling Location ²	Total		PLD ³ < 0.035			PLD > 0.035						
		n ⁴	RCS ⁵	n	RCS	Mean PLD (#/μm ²)	Mean Length (μm)	Mean Change in Si/(Si + Al) ⁶	n	RCS	Mean PLD (#/μm ²)	Mean Length (μm)	Mean Change in Si/(Si + Al)
CA	B	7	216	6	202	0.017	1.6	0.056	1	14	0.051	1.5	0.013 *
	P	4	162	2	78	0.021	1.8	0.053	2	84	0.039	1.6	0.008 *
	R	6	228	4	175	0.022	1.6	0.065	2	53	0.039	1.8	0.044
	F	7	191	7	191	0.018	1.7	0.071	0	0	-	-	-
	I	6	142	6	142	0.014	1.8	0.045	0	0	-	-	-
NA	B	3	132	3	132	0.011	1.5	0.070	0	0	-	-	-
	P	3	70	0	0	-	-	-	3	70	0.043	1.1	0.016 *
	R	4	111	3	88	0.021	1.5	0.054	1	23	0.056	1.4	0.014 *
	F	2	7	2	7	0.006	1.9	0.005 *	0	0	-	-	-
	I	3	24	3	24	0.004	1.8	0.081	0	0	-	-	-
MW	B	2	55	0	0	-	-	-	2	55	0.047	1.3	0.071
	P	1	43	0	0	-	-	-	1	43	0.038	1.1	0.048
	R	2	72	0	0	-	-	-	2	72	0.044	1.3	0.052
	F	3	79	2	49	0.021	1.9	0.079	1	30	0.049	1.4	0.066
	I	2	24	2	24	0.005	2.3	0.098	0	0	-	-	-
W	B	0	0	0	0	-	-	-	0	0	-	-	-
	P	0	0	0	0	-	-	-	0	0	-	-	-
	R	1	53	1	53	0.032	1.2	0.014 *	0	0	-	-	-
	F	1	27	1	27	0.015	1.2	0.056	0	0	-	-	-
	I	1	49	0	0	-	-	-	1	49	0.051	1.3	0.009 *
all Samples	B	12	403	9	334	0.015	1.6	0.062	3	69	0.048	1.3	0.059
	P	8	275	2	78	0.021	1.8	0.053	6	197	0.040	1.3	0.020 *
	R	13	464	8	316	0.023	1.5	0.053	5	148	0.044	1.5	0.044
	F	13	304	12	274	0.018	1.7	0.069	1	30	0.049	1.4	0.066
	I	12	239	11	190	0.012	1.9	0.057	1	49	0.051	1.3	0.009

¹ Mine region: CA = Central Appalachia; NA = northern Appalachia; MW = mid-west; W = west. ² Sampling location: B = roof bolter; P = production; R = return; F = feeder breaker; I = intake. ³ PLD: Particle loading density = number of particles/analyzed area (#/μm²) = can be converted to the standard #/m² by multiplying by a factor of 10¹²). ⁴ n = number of samples. ⁵ RCS = number of respirable crystalline silica particles. ⁶ Mean change in Si/(Si + Al) = the mean change in Si/(Si + Al) ratio between SEM–EDX measurements at 20 and 5 kV; values that fall within the established free silica thresholds (i.e., (−0.038, 0.036)) are denoted with *, and the rest of them are outside the free silica range.

3.1. Silica Particle Size

Figure 4 shows, as a function of the mine region and sampling location, the distribution of the particle length values observed for the individual particles analyzed by SEM–EDX using the procedure that is shown in Figure 2. The samples with a high PLD (i.e., PLD > 0.035 #/μm²) were excluded from the left column of plots, but all of the samples were included in the right column for comparison. Overall, the identified silica particles were somewhat finer in the samples from the P, B and R locations than in the samples from the F and I locations. This is consistent with expectations since the former locations are nearby to cutting or drilling activities which should produce relatively fine dust. Moreover, these results are consistent with silica size distributions that were generated from the pre-existing RCMD dataset available from Keles et al. [52]. Figure 5 shows the silica size distribution by sampling location for (a) the 58 RCMD samples analyzed for the current study, and (b) all of the 171 samples available from Keles et al. [52] and discussed by Sarver et al. [51]. Both of the plots indicate that respirable silica particles are finer in the P, B, and R locations.

With respect to the differences based on the mine region, Figure 5 shows that the identified silica particles were finer in the samples from the midwestern (MW) and western (W) mines than those from the Central (CA) and Northern Appalachian (NA) mines. This is also consistent with the observations from the pre-existing dataset (Figure 5c,d) and the data gathered from the CC routine used in the current study to identify the silica particles (see Figure S3). While this finding could challenge the notion that the respirable silica in the CA mines is particularly fine, it should be viewed in concert with the range of findings which show that the silica content (and mass and particle number concentration) is typically higher in CA than it is in the other regions (e.g., Doney et al. [11]; Agioutanti et al. [10]; Keles et al. [49]; Sarver et al. [51]). In other words, the respirable silica in the CA mines might not be quite as fine as it is in other mines, but it can be more abundant, and both of these factors should be important for considering the exposure risks. Furthermore, Figure 5e,f indicates that the respirable silica is generally finer than the other mineral types commonly observed in RCMD (i.e., aluminosilicates (AS) and carbonates (CB) (C and

MC are generally interpreted as coal dust particles in this size range, and thus, are not considered to be mineral particles).

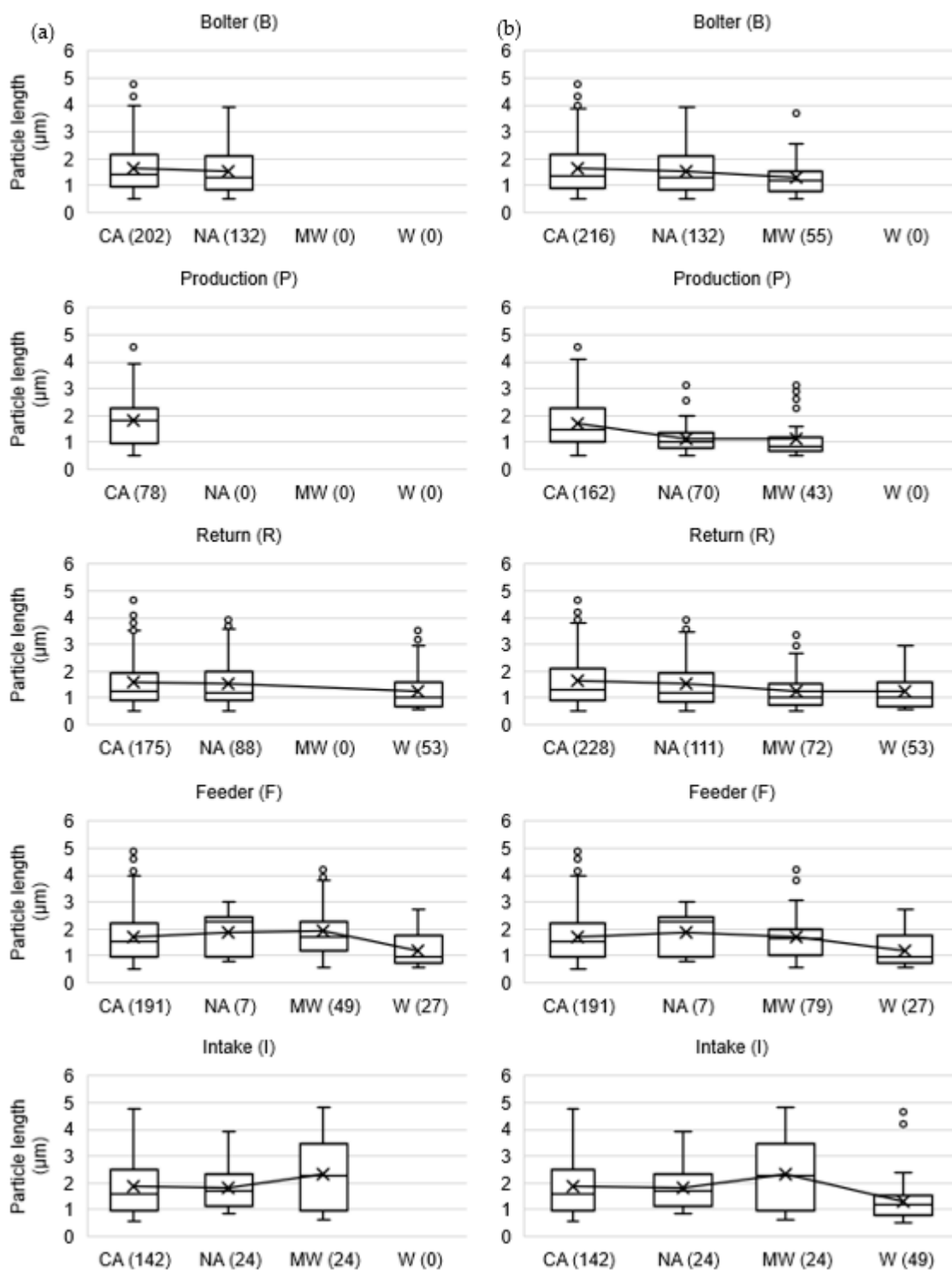


Figure 4. Distribution of silica particle size estimated from SEM-EDX data for the RCMD samples, with plots illustrated by mine region for each standardized sampling location. In (a), high-particle loading density (PLD) samples are excluded, while in (b), all of the samples are included regardless of PLD. Mine region: CA = Central Appalachia, NA = Northern Appalachia, MW = mid-west, W = west. Number of analyzed silica particles are given in parentheses. Small circles are outliers.

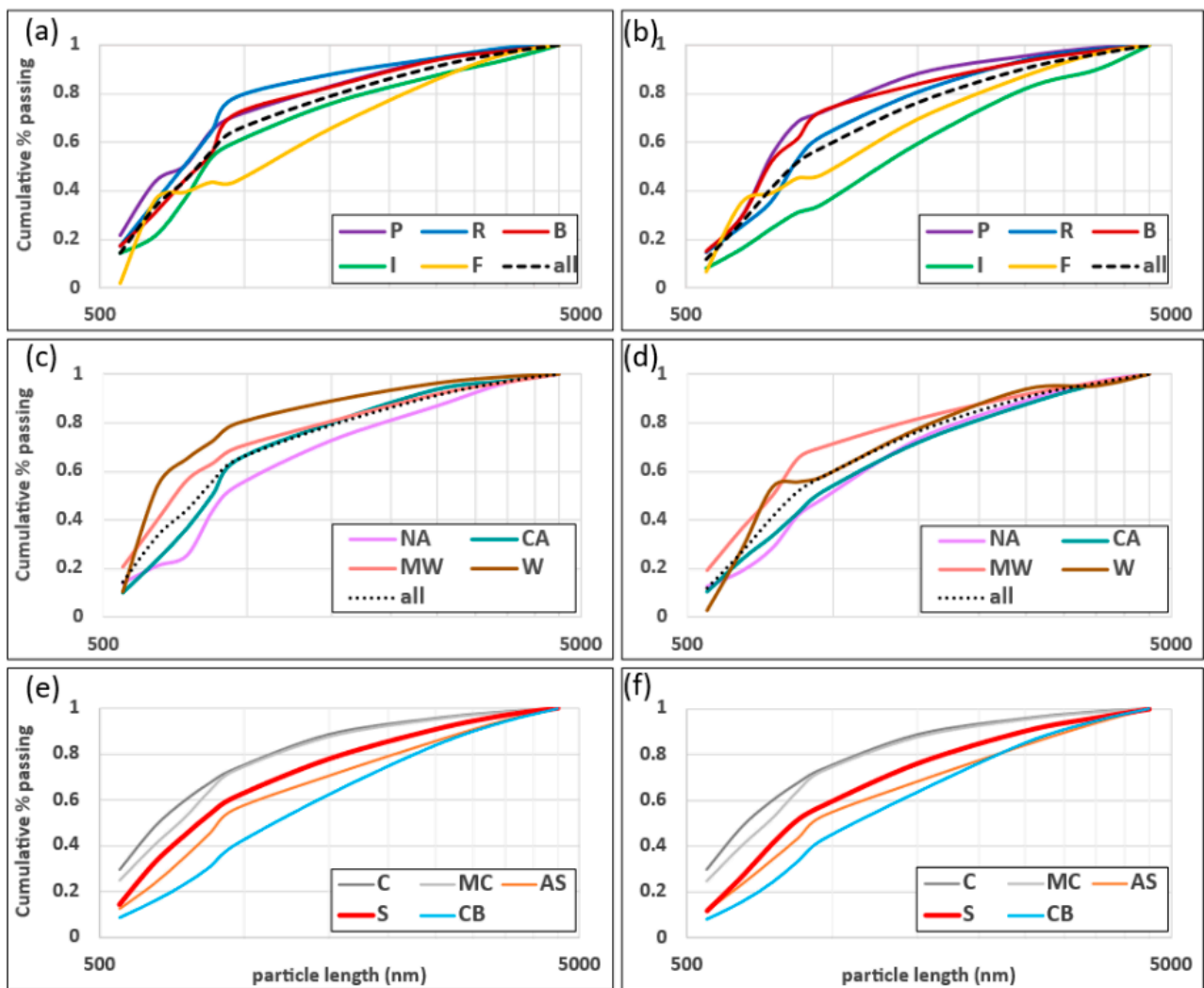


Figure 5. Overall size distribution plots for silica particles for the samples analyzed here for surface condition study, $n = 58$ (graphs on the left (i.e., a,c,e)) and all of the samples analyzed in [50,51], $n = 171$ (graphs on the right (i.e., b,d,f)); (a,b) in specific sampling locations (P = production, R = return, B = bolter, I = intake, F = feeder breaker); (c,d) in different mine regions (NA = northern Appalachia, CA = Central Appalachia, MW = mid-west, W = west); (e,f) relative to other mineralogy classes (S = silica, AS = aluminosilicates, C = carbonaceous, MC = mixed carbonaceous, and CB = carbonates). Data used to generate these plots are available from Keles et al. [52].

3.2. Silica Particle Surface Condition

As mentioned, the mean change in the $\text{Si}/(\text{Si} + \text{Al})$ ratio observed for the silica particles from 20 to 5 kV is summarized in Table 2. Figure 6 presents the distribution of change in the ratio values by the mine region and sampling location. Like the particle length plots in Figure 4, Figure 6 shows the results both with and without the high-PLD samples. Overall, the PLD does not appear to have much effect on the change in the ratio trends. The only visually discernable trend from Figure 6 is for the P location samples in the CA region, which suggests that inclusion of the high-PLD samples shifts the change in the $\text{Si}/(\text{Si} + \text{Al})$ distribution slightly downward. This probably due at least in part to interference of the nearby aluminosilicate particles when the EDX data were gathered from the target silica particles. Figure S4 summarizes $\text{Si}/(\text{Si} + \text{Al})$ as a function of PLD across all of the samples, and it clearly shows that silica particles identified in high PLD samples tend to have lower $\text{Si}/(\text{Si} + \text{Al})$ ratios at both 20 and 5 kV. This implies that some silica particles might have been completely missed in such samples during the silica identification procedure, i.e., because

they were sufficiently influenced by nearby Al-rich particles so that their Si/(Si + Al) ratio did not reach the 0.70 screening criteria at 15 kV.

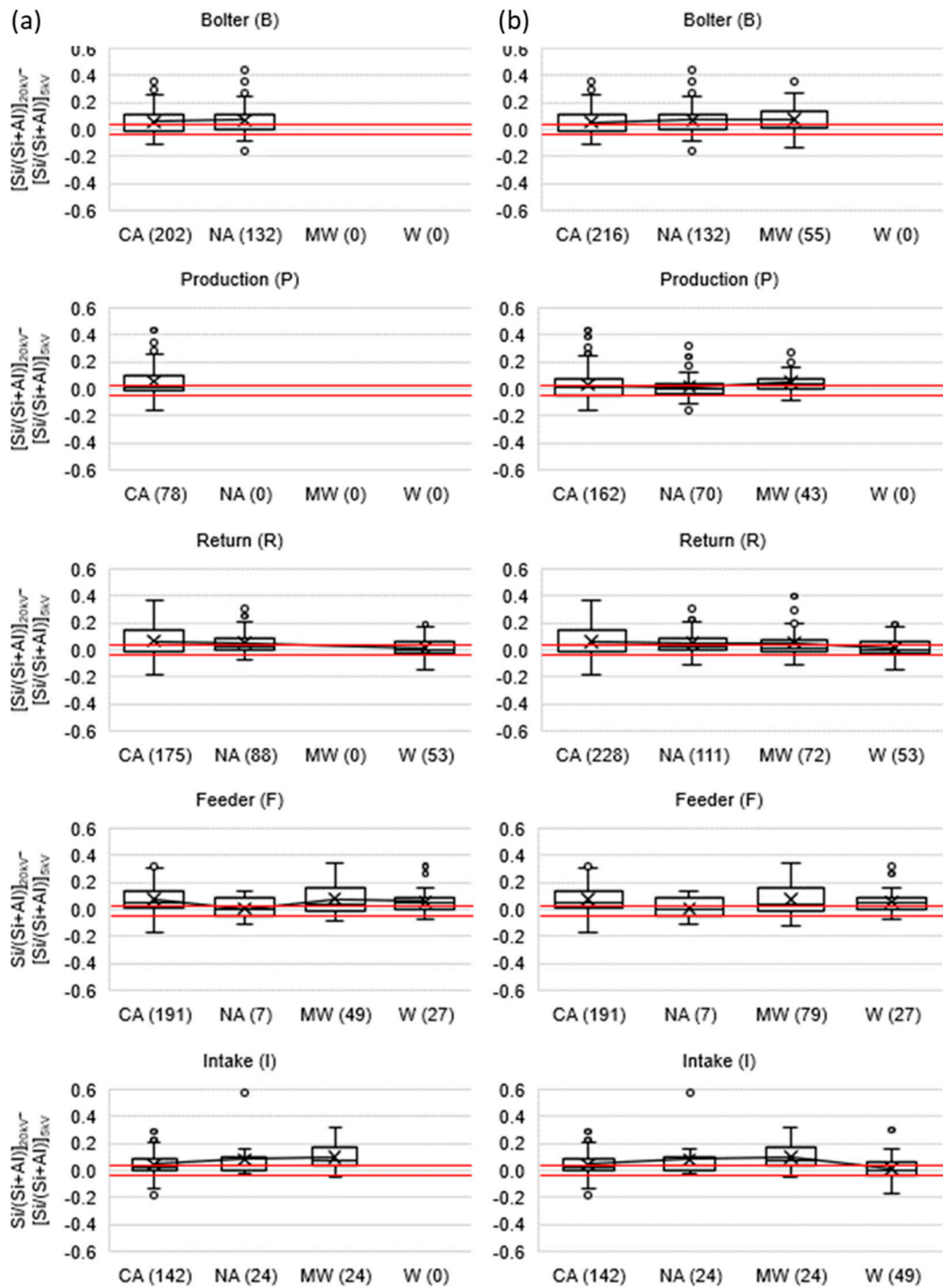


Figure 6. Distribution of the change in Si/(Si + Al) ratio between measurements at 20 and 5 kV for RCMD samples, with plots shown by mine region for each standardized sampling location. Red lines mark the free silica thresholds determined using the VCAS160 aluminosilicate glass powder reference material (i.e., (−0.038, 0.036)). Number of analyzed silica particles are given in parentheses. In (a), high-PLD samples are excluded, while in (b), all of the samples are included regardless of PLD. Small circles are outliers.

On the other hand, the distribution of change in the $\text{Si}/(\text{Si} + \text{Al})$ values was observed to gradually shift upward with the coarser particles (see Figure 7). This is probably an artifact of the analytical method. To explain, relative to the particle diameter, the 5 kV beam penetrates deeper into a fine particle than it does into a coarse particle. Thus, the EDX data captured for a coarser particle at 5 kV are a truer representation of the particle surface. Moreover, any indication that the silica surface condition differs by sampling location or mine might be influenced to some extent by the differences in particle size by location (e.g., as illustrated in Figure 4).

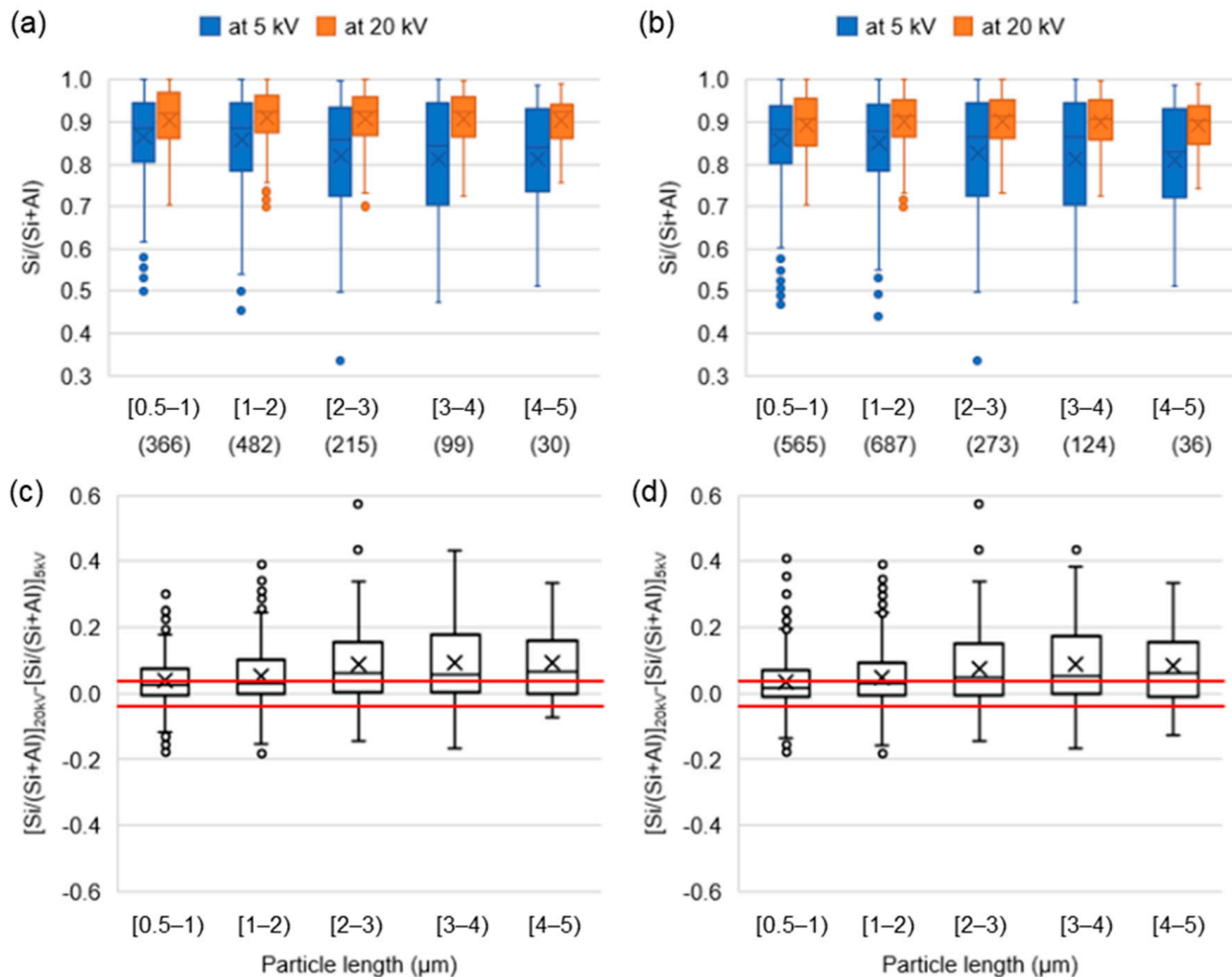


Figure 7. (a,b) show the distribution of the $\text{Si}/(\text{Si} + \text{Al})$ ratio at 20 and 5 kV as a function of particle length, while (c,d) show the distribution of the change in $\text{Si}/(\text{Si} + \text{Al})$ ratio between measurements at 20 and 5 kV as a function of particle length. Red lines mark the free silica thresholds determined using the VCAS160 aluminosilicate glass powder reference material (i.e., $(-0.038, 0.036)$). In (a,c), high-PLD samples are excluded, while in (b,d), all of the samples are included regardless of PLD. Number of analyzed silica particles are given in parentheses under particle lengths. Small circles are outliers.

The red lines in Figures 6 and 7 represent the thresholds for free silica classification (i.e., as established by the data derived from the VCAS160 control particles in Figure 3); the particles with values that fall between the red lines are interpreted as free silica. In general, free silica particles were observed more often in the samples from the NA and W region mines than in the samples from the CA and MW mines. Frost et al. [48] suggested that the relative abundance of free versus clay-occluded silica particles might be related to the specific sources of silica in a given mine. In the current study, it was generally

observed that mines which more rock cutting (i.e., relative to the total mining height) had somewhat fewer free silica particles (i.e., relative to total silica particles analyzed) than the mines with less rock cutting did (see Figure S5). However, it is impossible to know how much the mining conditions, geology or other local factors contributed to the observed differences given the above discussion of the effects of PLD and particle size. Rather, a more important observation from Figure 7 is the substantial variability in the respirable silica surface condition, with most of the particles falling outside of the free silica range.

Based on the conception of Wallace et al. [55], on which the analysis of the silica surface condition was based in the current work, the respirable silica particles should occur in two modes: free or clay-occluded. However, it must be noted that the seminal work by Wallace et al. [55] to distinguish between these two modes using the dual-voltage SEM–EDX analysis and the early application by Harrison et al. [44] for mine dust characterization differed from the current work in at least one significant way: they dispersed the particles prior to the analysis and/or they purposefully avoided the agglomerated particles during the analysis to enable the characterization of individual particles. Here, the particles were analyzed directly on the sample filter. While this approach has a clear drawback in terms of the PLD issue (i.e., PLD is difficult to control during sampling), it did allow for a characterization of the un-prepared particles, and indeed, some key observations in the current study indicate a wider range of silica occurrence modes in RCMD.

Per Figure 3, the change in Si/(Si + Al) ratio from 20 to 5 kV should ideally be either negligible (i.e., free silica) or sufficiently positive (i.e., occluded silica). As seen in Figure 7, though, there were a significant number of particles in the samples analyzed here that exhibited a negative change in the Si/(Si + Al) ratio. One explanation for this could simply be a partially occluded silica particle, for which the occluded surface just happened to be on the underside of the particle relative to its orientation on the sample filter (i.e., such that the EDX data at 20 kV could actually indicate a higher Al than the data could at 5 kV). Another explanation for this could be that the target silica particle occurs within an agglomerate that also contains clay particles.

As evidence of the range of respirable silica occurrences in the RCMD samples investigated here, Figure 8 presents a composite of SEM images captured during the silica particle surface analysis at 5 and 20 kV. In Figure 8, the imaged particles have been grouped into five categories by both their elemental data and their visual appearances: free silica, clay-occluded silica, micro-agglomerates containing silica (MAGs), silica ingrained within another particle and a silica particle with aluminosilicate interference. (More example images of respirable silica particles are presented in Figure S6, along with their change in the ratio. In general, it was observed that the silica particles which could be visually categorized as clay-occluded typically exhibited, as expected, a change in the Si/(Si + Al) > 0.036, and therefore, they would fall above the upper free silica threshold shown in Figures 6 and 7. Additionally, the silica particles ingrained within coal were observed to have some of the highest changes in the Si/(Si + Al) values. However, the silica particles observed within MAGs exhibited both positive and negative changes in the Si/(Si + Al) values, falling both above the upper and below the lower free silica thresholds).

In a binary classification scheme (i.e., free or clay-occluded) based only on the elemental data collected using the dual-voltage analysis, the particles in any of the four final categories in Figure 8 might exhibit a change in the Si/(Si + Al) ratio that would cause them to be classified as occluded. However, the images demonstrate a more complex reality, one where there are multiple manifestations of silica with surface-associated clays (and other particle types). Indeed, it is the combination of elemental data and visual appearance that enables a complete interpretation of the particle type. Importantly, while the final category in Figure 8 is an artifact of over-sampling (i.e., leading to a high PLD such that the silica particle could not be reliably characterized by the dual-voltage SEM–EDX analysis), the presence of MAGs and ingrained particles represent additional possibilities for respirable silica occurrence that have heretofore not been widely considered.

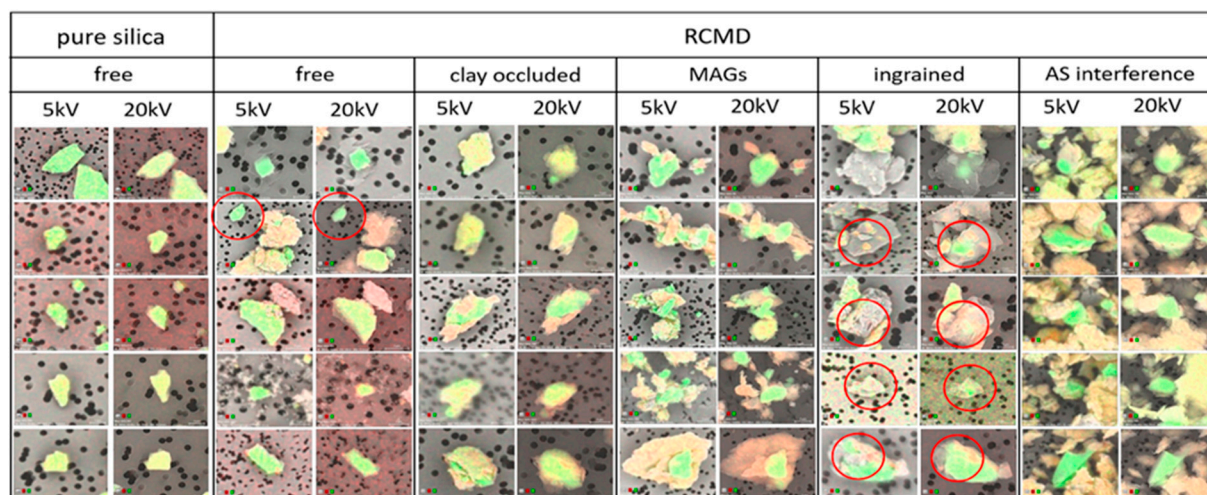


Figure 8. Example SEM images with elemental mapping of Si (green) and Al (red) that show silica particles with various other manifestations of surface-associated clay particles. Respirable silica particles in pure free silica category were collected from the Min-U-Sil 5 (1st row), Sil-Co-Sil (2nd and 3rd rows) and VCAS160 (4th and 5th rows) reference materials. Respirable silica particles in RCMD were collected from some of the 58 samples included in current study.

Since the images were not captured for all of the particles analyzed in this study, the frequency of their occurrence in each category cannot be determined. However, anecdotally, MAGs were common, and they could include the particles that were classified as free silica or clay-occluded based on their change in the Si/(Si + Al) ratio. For the RCMD samples studied here, it is impossible to say whether the MAGs existed as such in the mine environment or whether they were formed as an artifact of the sample collection procedure. However, a recent study demonstrated that MAGs can be formed due to dust generation processes and/or a high concentration environment [59]. In that study, the dust was generated by grinding raw coal and rock materials in the laboratory, and the samples were collected passively (i.e., without an air pump, cyclone or tubing) for a direct-on-filter SEM–EDX analysis. Further, the replicate samples were subjected to brief sonication and/or a simulated lung surfactant to explore their dispersibility. If respirable silica does frequently occur as MAGs in mines or other occupational environments, that knowledge could be important for informing the conceptual models of exposure and the interpretation of the lung response, not to mention for monitoring technologies specifically aimed at silica. Passive sampling in the mine environment could be a feasible method to confirm and characterize MAG occurrence.

4. Conclusions

A better understanding of respirable silica characteristics is critical for identifying the exposure risks and targeting more effective dust monitoring and control strategies in coal mines. In the current work, 58 respirable coal mine dust samples were analyzed by SEM–EDX from the mines in four different geographic regions. The results showed that silica particles, like other dust particles, are relatively finer near the sources of active dust generation due to mining or drilling into the geologic strata, and the previous work on the same samples showed that the silica is primarily sourced from the rock strata in most of the mines [48]. Individual silica particles were also interrogated at two different voltages with the intent to classify them as either “free” or “clay-occluded”—with the latter perhaps posing less severe hazards for lung health. However, the direct-on-filter analysis in this work proved challenging. Some of the samples exhibited high particle loading density such that nearby clay particles might interfere with the silica analysis. Moreover, many silica particles were observed to occur in modes other than free or clay-occluded, most notably within (respirable sized) micro-agglomerates that contained the silica along

with other particles. Occasionally, the silica particles also appeared to be ingrained within other particles (e.g., coal). These findings shed new light on the range of possible modes of occurrence of respirable silica in mines, and they should be valuable both for those considering exposure outcomes and monitoring techniques.

Future work to investigate respirable particle silica surfaces and their modes of occurrence may benefit from additional analyses and additional analytical tools. For example, using the dual-voltage SEM–EDX method as in the current study, the analysis of the dust particles before and after a dispersion step could help to elucidate the presence and persistence of micro-agglomerates. To more definitively demonstrate the presence of clay-occluded silica, tools such as transmission electron microscopy, Raman spectroscopy or micro-computed tomography could be helpful.

Supplementary Materials: The following supporting information can be downloaded at: <https://www.mdpi.com/article/10.3390/min12121555/s1>, Figure S1: Schematic diagrams illustrating approximate sampling locations for RCMD samples in (a) continuous miner and (b) longwall mine operations; Figure S2: Distribution of silica particle size estimated from SEM–EDX data for the RCMD samples for various particle loading density ranges; Figure S3: Overall size distributions for silica particles using data collected from the CC SEM–EDX routine established for silica particle identification for this study; Figure S4: (a) Distribution of the Si/(Si + Al) ratio at 20 and 5 kV as a function of PLD across all samples, and (b) distribution of the change in Si/(Si + Al) ratio between measurements at 20 and 5 kV as a function of PLD across all of the samples; Figure S5: Distribution of the change in Si/(Si + Al) ratio between measurements at 20 and 5 kV per mine across all samples; Figure S6: Some example particles, organized by the change in Si/(Si + Al) ratio at 5 and 20 kV; Table S1: The individual silica particle data for each sample.

Author Contributions: Conceptualization, E.S. and C.K.; methodology, C.K. and E.S.; validation, C.K.; formal analysis, C.K.; investigation, E.S. and C.K.; resources, E.S.; writing—original draft preparation, C.K.; writing—review and editing, E.S., and C.K.; supervision, E.S.; project administration, E.S. and C.K.; funding acquisition, E.S. All authors have read and agreed to the published version of the manuscript.

Funding: This research was funded by National Institute for Occupational Safety and Health (NIOSH), grant number 75D30119C05528.

Data Availability Statement: Not applicable.

Acknowledgments: The authors would like to thank NIOSH for funding this work. We kindly acknowledge our industry partners and mine personnel for arranging mine access and providing logistical support with the dust sampling. The SEM–EDX work presented here was performed in part at the Nanoscale Characterization and Fabrication Laboratory, which is supported by the Virginia Tech National Center for Earth and Environmental Nanotechnology Infrastructure (NanoEarth), a member of the National Nanotechnology Coordinated Infrastructure (NNCI), supported by NSF (ECCS 1542100 and ECCS 2025151). We want to thank Steve McCartney of ICTAS-NCFL for assistance with SEM–EDX work. We also thank Alex Norris, Kyle Louk, Eleftheria Agioutanti, Lizeth Jaramillo, Jonathan Gonzalez, Nishan Pokhrel, Baxter Jones and Setareh Afrouz for their assistance with the dust sampling. The views, opinions and recommendations expressed herein are solely those of the authors and do not imply any endorsement by the funding source or research partners.

Conflicts of Interest: The authors declare no conflict of interest. The funders had no role in the design of the study; in the collection, analyses, or interpretation of data; in the writing of the manuscript, or in the decision to publish the results.

References

1. Hall, N.B.; Blackley, D.J.; Halldin, C.N.; Laney, A.S. Current review of pneumoconiosis among US coal miners. *Curr. Environ. Health Rep.* **2019**, *6*, 137–147. [[CrossRef](#)] [[PubMed](#)]
2. Antao, V.C.D.S.; Petsonk, E.L.; Sokolow, L.; Wolfe, A.L.; Pinheiro, G.A.; Hale, J.M.; Attfield, M.D. Rapidly progressive coal workers' pneumoconiosis in the United States: Geographic clustering and other factors. *Occup. Environ. Med.* **2005**, *62*, 670–674. [[CrossRef](#)] [[PubMed](#)]

3. Laney, A.S.; Weissman, D.N. Respiratory diseases caused by coal mine dust. *J. Occup. Environ. Med.* **2014**, *56*, S18–S22. [[CrossRef](#)] [[PubMed](#)]
4. Hall, N.B.; Blackley, D.J.; Halldin, C.N.; Laney, A.S. Continued increase in prevalence of r-type opacities among underground coal miners in the USA. *Occup. Environ. Med.* **2019**, *76*, 479–481. [[CrossRef](#)]
5. Laney, A.S.; Petsonk, E.L.; Attfield, M.D. Pneumoconiosis among underground bituminous coal miners in the United States: Is silicosis becoming more frequent? *Occup. Environ. Med.* **2010**, *67*, 652–656. [[CrossRef](#)] [[PubMed](#)]
6. Cohen, R.A.; Petsonk, E.L.; Rose, C.; Young, B.; Regier, M.; Najmuddin, A.; Abraham, J.L.; Chung, A.; Green, F.H.Y. Lung Pathology in U.S. Coal Workers with Rapidly Progressive Pneumoconiosis Implicates Silica and Silicates. *Am. J. Respir. Crit. Care Med.* **2016**, *193*, 673–680. [[CrossRef](#)]
7. Cohen, R.A.; Rose, C.S.; Go, L.H.T.; Zell-Baran, L.M.; Almborg, K.S.; Sarver, E.A.; Lowers, H.A. Pathology and mineralogy demonstrate respirable crystalline silica is a major cause of severe pneumoconiosis in U.S. coal miners. *Ann. Am. Thorac. Soc.* **2022**, *19*, 1469–1478. [[CrossRef](#)]
8. Jelic, T.M.; Estelilla, O.C.; Sawyer-Kaplan, P.R.; Plata, M.J.; Powers, J.T.; Emmett, M.; Kuenstner, J.T. Coal mine dust desquamative chronic interstitial pneumonia: A precursor of dust-related diffuse fibrosis and of emphysema. *Int. J. Occup. Environ. Med.* **2017**, *8*, 153–165. [[CrossRef](#)]
9. National Academies of Sciences, Engineering, and Medicine. *Monitoring and Sampling Approaches to Assess Underground Coal Mine Dust Exposures*; The National Academies Press: Washington, DC, USA, 2018. [[CrossRef](#)]
10. Agioutanti, E.; Keles, C.; Sarver, E. A thermogravimetric analysis application to determine coal, carbonate, and non-carbonate minerals mass fractions in respirable mine dust. *J. Occup. Environ. Hyg.* **2020**, *17*, 47–58. [[CrossRef](#)]
11. Doney, B.C.; Blackley, D.; Hale, J.M.; Halldin, C.; Kurth, L.; Syamlal, G.; Laney, A.S. Respirable coal mine dust in underground mines, United States, 1982–2017. *Am. J. Ind. Med.* **2019**, *62*, 478–485. [[CrossRef](#)]
12. Mischler, S.E.; Cauda, E.G.; Di Giuseppe, M.; McWilliams, L.J.; Croix, C.S.; Sun, M.; Franks, J.; Ortiz, L.A. Differential activation of RAW 264.7 macrophages by size-segregated crystalline silica. *J. Occup. Med. Toxicol.* **2016**, *11*, 57. [[CrossRef](#)] [[PubMed](#)]
13. Ohyama, M.; Tachi, H.; Minejima, C.; Kameda, T. Comparing the role of silica particle size with mineral fiber geometry in the release of superoxide from rat alveolar macrophages. *J. Toxicol. Sci.* **2014**, *39*, 551–559. [[CrossRef](#)] [[PubMed](#)]
14. Wiessner, J.H.; Mandel, N.S.; Sohnle, P.G.; Mandel, G.S. Effect of particle size on quartz-induced hemolysis and on lung-inflammation and fibrosis. *Exp. Lung Res.* **1989**, *15*, 801–812. [[CrossRef](#)]
15. Goldstein, B.; Webster, I. Intratracheal injection into rats of size-graded silica particles. *Br. J. Ind. Med.* **1966**, *23*, 71–74. [[CrossRef](#)] [[PubMed](#)]
16. IARC. Silica, Some Silicates, Coal Dust and Para-Aramid Fibrils. In *Monographs on the Evaluation of Carcinogenic Risks to Humans*; IARC: Lyon, France, 1997; Volume 68.
17. Vallyathan, V.; Shi, X.L.; Dalal, N.S.; Irr, W.; Castranova, V. Generation of free radicals from freshly fractured silica dust. Potential role in acute silica-induced lung injury. *Am. Rev. Respir. Dis.* **1988**, *138*, 1213–1219. [[CrossRef](#)] [[PubMed](#)]
18. Meldrum, M.; Howden, P. Crystalline silica: Variability in fibrogenic potency. *Ann. Occup. Hyg.* **2002**, *46*, 27–30. [[CrossRef](#)]
19. Leung, C.C.; Yu, I.T.S.; Chen, W. Silicosis. *Lancet* **2012**, *379*, 2008–2018. [[CrossRef](#)]
20. Hoy, R.F.; Chambers, D.C. Silica-related diseases in the modern world. *Allergy* **2020**, *75*, 2805–2817. [[CrossRef](#)]
21. Hamilton, R.F., Jr.; Thakur, S.A.; Holian, A. Silica binding and toxicity in alveolar macrophages. *Free Radic. Biol. Med.* **2008**, *44*, 1246–1258. [[CrossRef](#)]
22. Borm, P.J.A.; Fowler, P.; Kirkland, D. An updated review of the genotoxicity of respirable crystalline silica. *Part Fibre. Toxicol.* **2018**, *15*, 23. [[CrossRef](#)]
23. Greenberg, M.I.; Waksman, J.; Curtis, J. Silicosis: A Review. *Dis Mon.* **2007**, *53*, 394–416. [[CrossRef](#)] [[PubMed](#)]
24. Page, S.J. Comparison of coal mine dust size distributions and calibration standards for crystalline silica analysis. *Am. Ind. Hyg. Assoc. J.* **2003**, *64*, 30–39. [[CrossRef](#)] [[PubMed](#)]
25. Chubb, L.; Cauda, E. Characterizing particle size distributions of crystalline silica in gold mine dust. *Aerosol. Air Qual. Res.* **2017**, *17*, 24–33. [[CrossRef](#)] [[PubMed](#)]
26. Chisholm, W.P.; Lee, T.; Chirila, M. Determination of crystalline silica in dust at low concentrations by low-temperature infrared spectrometry. *Annu. Book ASTM Stand Sect. 11 Water Environ. Technol.* **2013**, *2013*, 1–11. [[CrossRef](#)]
27. Sarver, E.; Keles, C.; Rezaee, M. Beyond conventional metrics: Comprehensive characterization of respirable coal mine dust. *Int. J. Coal Geol.* **2019**, *207*, 84–95. [[CrossRef](#)]
28. Sarver, E.; Keles, C.; Rezaee, M. Characteristics of respirable dust in eight Appalachian coal mines: A dataset including particle size and mineralogy distributions, and metal and trace element mass concentrations. *Data Br.* **2019**, *25*, 104032. [[CrossRef](#)]
29. Rendall, R.E.G.; Goldstein, B.; Coetzee, F.S.J. Importance of particle size in the development of silicosis. *Suid Afr. J. Sci.* **1988**, *84*, 125–128.
30. Monteiller, C.; Tran, L.; MacNee, W.; Faux, S.; Jones, A.; Miller, B.; Donaldson, K. The pro-inflammatory effects of low-toxicity low-solubility particles, nanoparticles and fine particles, on epithelial cells in vitro: The role of surface area. *Occup. Environ. Med.* **2007**, *64*, 609–615. [[CrossRef](#)]
31. Gwinn, M.R.; Leonard, S.S.; Sargent, L.M.; Lowry, D.T.; McKinstry, K.; Meighan, T.; Reynolds, S.H.; Kashon, M.; Castranova, V.; Vallyathan, V. The role of p53 in silica-induced cellular and molecular responses associated with carcinogenesis. *J. Toxicol. Environ. Health A* **2009**, *72*, 1509–1519. [[CrossRef](#)]

32. Vallyathan, V.; Kang, J.H.; Van Dyke, K.; Dalal, N.S.; Castranova, V. Response of alveolar macrophages to in vitro exposure to freshly fractured versus aged silica dust: The ability of Prosil 28, an organosilane material, to coat silica and reduce its biological reactivity. *J. Toxicol. Environ. Health* **1991**, *33*, 303–315. [[CrossRef](#)]
33. Castranova, V.; Pailes, W.H.; Dalal, N.S.; Miles, P.R.; Bowman, L.; Vallyathan, V.; Pack, D.; Weber, K.C.; Hubbs, A.; Schwegler-Berry, D.; et al. Enhanced pulmonary response to the inhalation of freshly fractured silica as compared with aged dust exposure. *Appl. Occup. Environ. Hyg.* **1996**, *11*, 937–947. [[CrossRef](#)]
34. Vallyathan, V.; Castranova, V.; Pack, D.; Leonard, S.; Shumaker, J.; Hubbs, A.F.; Shoemaker, D.A.; Ramsey, D.M.; Pretty, J.R.; McLaurin, J.L.; et al. Freshly fractured quartz inhalation leads to enhanced lung injury and inflammation. Potential role of free radicals. *Am. J. Respir. Crit. Care Med.* **1995**, *152*, 1003–1009. [[CrossRef](#)] [[PubMed](#)]
35. Gothe, C.J.; Lidstrom, L.; Swensson, A. Influence of mode of disintegration on the fibrogenetic power of quartz particles. *Med. Lav.* **1971**, *62*, 375–377.
36. Fubini, B. Surface chemistry and quartz hazard. *Ann. Occ. Hyg.* **1998**, *42*, 521–530. [[CrossRef](#)] [[PubMed](#)]
37. Chen, W.; Hnizdo, E.; Chen, J.Q.; Atfield, M.D.; Gao, P.; Hearl, F.; Lu, J.; Wallace, W.E. Risk of silicosis in cohorts of Chinese tin and tungsten miners and pottery workers (I): An epidemiological study. *Am. J. Ind. Med.* **2005**, *48*, 1–9. [[CrossRef](#)]
38. Creutzenberg, O.; Hansen, T.; Ernst, H.; Muhle, H.; Oberdörster, G.; Hamilton, R. Toxicity of a quartz with occluded surfaces in a 90-day intratracheal instillation study in rats. *Inhal. Toxicol.* **2008**, *20*, 995–1008. [[CrossRef](#)]
39. Stone, V.; Jones, R.; Rollo, K.; Duffin, R.; Donaldson, K.; Brown, D.M. Effect of coal mine dust and clay extracts on the biological activity of the quartz surface. *Toxicol. Lett.* **2004**, *149*, 255–259. [[CrossRef](#)]
40. Ziemann, C.; Harrison, P.T.; Bellmann, B.; Brown, R.C.; Zoitos, B.K.; Class, P. Lack of marked cyto- and genotoxicity of cristobalite in devitrified (heated) alkaline earth silicate wools in short-term assays with cultured primary rat alveolar macrophages. *Inhal. Toxicol.* **2014**, *26*, 113–127. [[CrossRef](#)]
41. Mestres, G.; Espanol, M.; Xia, W.; Tenje, M.; Ott, M. Evaluation of biocompatibility and release of reactive oxygen species of aluminum oxide-coated materials. *ACS Omega* **2016**, *1*, 706–713. [[CrossRef](#)]
42. Ziemann, C.; Escrig, A.; Bonvicini, G.; Ibáñez, M.J.; Monfort, E.; Salomoni, A.; Creutzenberg, O. Organosilane-based coating of quartz species from the traditional ceramics industry: Evidence of hazard reduction using in vitro and in vivo tests. *Ann. Work Expo. Health* **2017**, *61*, 468–480. [[CrossRef](#)]
43. Duffin, R.; Gilmour, P.S.; Schins, R.P.F.; Clouter, A.; Guy, K.; Brown, D.M.; MacNee, W.; Borm, P.J.; Donaldson, K.; Stone, V. Aluminum lactate treatment of DQ12 quartz inhibits its ability to cause inflammation, chemokine expression, and nuclear factor- κ B activation. *Toxicol. Appl. Pharmacol.* **2001**, *176*, 10–17. [[CrossRef](#)] [[PubMed](#)]
44. Walton, W.H.; Dodgson, J.; Hadden, G.G.; Jacobsen, M. The effect of quartz and other non-coal dusts in coal workers' pneumoconiosis. In *Inhaled Particles IV*; Walton, W.H., Ed.; Unwin Brothers Ltd.: Surrey, UK, 1977; Volume 2, pp. 669–689.
45. Harrison, J.C.; Brower, P.S.; Atfield, M.D.; Doak, C.B.; Keane, M.J.; Grayson, R.L.; Wallace, W.E. Surface composition of respirable silica particles in a set of US anthracite and bituminous coal mine dusts. *J. Aerosol. Sci.* **1997**, *28*, 689–696. [[CrossRef](#)]
46. Wallace, W.E.; Harrison, J.C.; Grayson, R.L.; Keane, M.J.; Bolsaitis, P.; Kennedy, R.D.; Wearden, A.Q.; Atfield, M.D. Aluminosilicate surface contamination of respirable quartz particles from coal mine dusts and from clay works dusts. *Ann. Occup. Hyg.* **1994**, *38*, 439–445. [[CrossRef](#)]
47. Wallace, W.E.; Chen, J.; Harrison, J.; Hnizdo, V.; Chen, W.; Nelson, J.; Chisholm, W.; Hnizdo, E.; Keane, M.J.; Miller, W.E. Respirable silica particle occlusion by aluminosilicate: Surface properties of dusts with disease risk anomalies. *Med. Lav.* **2002**, *93*, S66–S67.
48. Frost, L.; Keles, C.; Sarver, E. A preliminary investigation of respirable silica particle surfaces in central Appalachian coal mine dust. In Proceedings of the 17th North American Mine Ventilation Symposium, Montreal, QC, Canada, 1 May 2019.
49. Keles, C.; Pokhrel, N.; Sarver, E. A study of respirable silica in underground coal mines: Sources. *Minerals* **2022**, *12*, 1115. [[CrossRef](#)]
50. Code of Federal Regulations (CFR). Mineral Resources. In *Mandatory Safety Standards-Underground Coal Mines*; Office of the Federal Register: Washington, DC, USA, 1969.
51. Sarver, E.; Keles, C.; Afrouz, S.G. Particle size and mineralogy distributions in respirable dust samples from 25 US underground coal mines. *Int. J. Coal Geol.* **2021**, *247*, 103851. [[CrossRef](#)]
52. Keles, C.; Tabora, M.J.; Sarver, E. Updating “Characteristics of respirable dust in eight Appalachian coal mines: A dataset including particle size and mineralogy distributions, and metal and trace element mass concentrations” with expanded data to cover a total of 25 US mines. *Data Br.* **2022**, *42*, 108125. [[CrossRef](#)]
53. Goldstein, J.I.; Newbury, D.E.; Echlin, P.; Joy, D.C.; Lyman, C.E.; Lifshin, E.; Sawyer, L.; Michael, J.R. Procedures for elimination of charging in nonconducting specimens. In *Scanning Electron Microscopy and X-Ray Microanalysis*, 3rd ed.; Goldstein, J.I., Newbury, D.E., Eds.; Springer: New York, NY, USA, 2003; pp. 647–673.
54. Harrison, J.; Chen, J.Q.; Miller, W.; Chen, W.; Hnizdo, E.; Lu, J.; Chisholm, W.; Keane, M.; Gao, P.; Wallace, W. Risk of silicosis in cohorts of Chinese tin and tungsten miners and pottery workers (II): Workplace-specific silica particle surface composition. *Am. J. Ind. Med.* **2005**, *48*, 10–15. [[CrossRef](#)]
55. Wallace, W.E.; Harrison, J.; Keane, M.J.; Bolsaitis, P.; Eppelsheimer, D.; Poston, J.; Page, S.J. Clay occlusion of respirable quartz particles detected by low voltage scanning electron microscopy-X-ray analysis. *Ann. Occup. Hyg.* **1990**, *34*, 195–204. [[CrossRef](#)]

56. Wallace, W.E.; Keane, M.J. Differential Surface Composition Analysis by Multiple-Voltage Electron Beam X-ray Spectrometry. US Patent 5,210,414, 11 May 1993.
57. Hnizdo, V.; Wallace, W.E. Monte Carlo analysis of the detection of clay occlusion of respirable quartz particles using multiple voltage scanning electron microscopy. *Scanning* **2002**, *24*, 264–269. [[CrossRef](#)]
58. Pokhrel, N.; Agioutanti, E.; Keles, C.; Afrouz, S.; Sarver, E. Comparison of respirable coal mine dust constituents estimated using FTIR, TGA, and SEM-EDX. *MMEX* **2022**, *39*, 291–300. [[CrossRef](#)]
59. Gonzalez, J.; Keles, C.; Sarver, E. On the occurrence and persistence of coal-mineral microagglomerates in respirable coal mine dust. *MMEX* **2022**, *39*, 271–282. [[CrossRef](#)]